

Injected and Leaked: Actively Inducing Side-Channel Leakage Using Electromagnetic Injection and Hardware Nonlinearity

Haoran Yan¹, Ziyu Shao¹, Shuhao Zhang¹, Qinhong Jiang^{2†}, Yan Long^{1†}

¹The Hong Kong University of Science and Technology (Guangzhou)

²The Hong Kong Polytechnic University

{hyan097, szhang515}@connect.hkust-gz.edu.cn; ziyushao@hkust-gz.edu.cn
qinhong.jiang@polyu.edu.hk; yanlong@hkust-gz.edu.cn

Abstract

Electromagnetic (EM) side-channel leakage and injection are typically treated as distinct physical phenomena, threatening data confidentiality and integrity respectively. This work investigates how EM injection can be used to amplify side-channel leakage that is otherwise infeasible. We introduce a novel framework for *Injection-Induced EM Side Channels* to enable integrated, closed-loop EM security analysis. Our theoretical modeling and experimental measurements reveal that nonlinear hardware components, such as ubiquitous amplifiers, analog-to-digital converters, and power converters, can modulate secret electrical signals onto an injected EM carrier and thus upconvert low-frequency secrets into measurable EM emissions. By tuning the injection frequency and amplitude, adversaries gain the ability to actively shape the effective spectrum and entropy of the resulting leakage. We design *InjectEave* attack and demonstrate eavesdropping on the audio played through wired and wireless headphones from up to 30 m away with accessible RF equipment, as well as in through-wall scenarios, and characterize injection-induced EM leakage of other low-frequency secrets such as power consumption of smart home devices and analog sensor inputs. Case studies further demonstrate how the proposed techniques enable closed-loop eavesdropping and manipulation of landline-phone conversations. Finally, we analyze the broader security challenges and mitigations.

1 Introduction

This work investigates the new problem statement of exploiting active electromagnetic (EM) injection and the inherent nonlinearity of computer hardware to reshape the capability of conventional electromagnetic side-channel analysis. Side-channel analysis has become one of the most important types of security analysis methodologies, exploiting the non-ideal abstractions of computer systems to compromise confidentiality and achieve unauthorized access to data internal to a

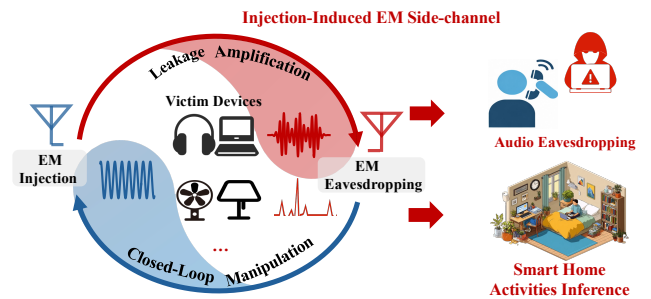


Figure 1: Injection-induced EM Side Channel utilizes active EM injection and ubiquitous hardware nonlinearity to produce controllable EM leakage, enabling unconventional EM eavesdropping vectors against low-frequency analog secrets.

protected device [3, 65]. By collecting and analyzing signals unintentionally produced by the physical operations of computer hardware, such as sound [4, 7, 9, 42], light [17, 44, 45], and electromagnetic emissions [32, 41, 73], adversaries would be able to infer critical information of cryptographic operations [11, 18, 19], confidential input data [9, 20, 27], and private user identity [36, 37, 41, 52].

Among various methods of side channels, EM side channels present a highly pervasive and impactful attack surface, as all modern computer systems rely on current and voltage variations in electrical circuits to perform all computations. The resulting time-varying EM fields inevitably radiate into the surrounding environment and propagate through the air to nearby adversaries. For example, the security community has shown the feasibility of exploiting EM side-channel leakage to eavesdrop on a wide range of secret information, such as screen displays [33, 40], keyboard and touchscreen interactions [27, 73], users’ biometrics [37, 52, 81], and even confidential video streams of smart home cameras [41].

Despite the massive theoretical attack surface, existing EM side-channel research has revealed a critical limitation in the range of applicable eavesdropping distances and observable types of information, especially on secrets in the form of low-

[†] Corresponding authors.

frequency analog signals. Specifically, the EM energy that can propagate to external adversaries is solely determined by the target’s internal characteristics, including the amplitude of the current/voltage that carries the secret information, the frequency of the internal electrical signals, and the EM transfer efficiency of the target’s circuits that act as unintentional radiating antennas. This major limitation is rooted in the threat model assumption that the side-channel analyzer can only passively observe the EM leakage of a target device. As a result, *conventional passive side-channel eavesdroppers face the seemingly “unsolvable” problem of low signal-to-noise ratio (SNR)*, treating better EM receivers as their only measure for improving EM side-channel capabilities.

Toward overcoming this challenge, this work rethinks the passive eavesdropping paradigm and provides a new analytical framework that employs active EM injection to induce and amplify EM side-channel leakage of analog electrical signals in controllable ways. The key insight behind our approach is that a fundamental frequency mismatch between internal secret signals and the circuit’s efficient EM coupling bands creates a physical barrier, significantly limiting the secret energy that can *leave* the device. Meanwhile, we observe that existing injection research [26, 35, 69] has shown how external EM signals can be designed to be at the most efficient coupling frequencies to *enter* the target device. Importantly, injected EM signals could be unintentionally demodulated by nonlinear hardware such as amplifiers, allowing adversaries to use EM carriers to inject false *low-frequency analog signals* into target systems. This is related to the recent concept of active side-channel analysis, where adversaries generate signals to illuminate a device and analyze the reflected response to recover digital data such as serial bits [29, 58] or cryptographic information [30, 49]. However, such a reflection-based impedance-change model is limited to coarse-grained binary impedance-state analysis and cannot characterize waveform-level leakage of continuous analog secrets.

Building upon these works and the significant existing gaps, we formulate *Injection-Induced EM Side Channel*. Unlike reflection-based approaches, our method characterizes how internal electrical signals are modulated onto an injected carrier through hardware nonlinearity and subsequently converted into secret-bearing EM leakage. This bridges the theoretical and experimental gaps between side-channel leakage and EM injection, establishing the physical basis for injection-induced eavesdropping, even for ubiquitous analog signals. We hypothesize that *nonlinear computer hardware can modulate analog secret information, in the form of electrical inputs of these hardware components, onto injected carriers, which could then emit and propagate back to side-channel eavesdroppers*.

If this hypothesis were true, then EM side-channel eavesdroppers would be able to actively control their injected EM carriers to break through the target devices’ EM security boundaries. We characterize this threat model with experiments on four types of the most typical nonlinear hardware

components found in computer systems, including amplifiers, analog-to-digital converters, power converters, and switching MOSFETs. Our measurements verify that injection-induced side channels enable unconventional attack vectors, such as eavesdropping on secret information with EM frequencies on the order of 10 Hz–10 kHz, which itself could be too low to propagate to external eavesdroppers. Our theoretical modeling further provides a framework for analyzing threats against the most common analog data interfaces, such as audio output and input, control signals of actuators, and even device power traces (Fig. 1).

Despite these new capabilities, our tests show that signals eavesdropped with this approach unavoidably suffer from higher-order inter-modulation that adds harmonics of an original signal to its spectrum. This nonlinearity-specific distortion poses unique challenges to eavesdroppers who aim to recover wideband signals, such as human speech audio. We design *InjectEave* to recover higher-fidelity secrets. *InjectEave* utilizes a diffusion-based denoising model and training data simulated by our developed quantitative model. Tests on physically collected speech audio data show notable improvements in several audio quality metrics.

Our evaluation in lab settings first identifies typical low-frequency analog secrets carried by 11 commercial off-the-shelf (COTS) household devices. Audio of headphones and landline phones could leak both speaker identity and spoken content. Control signals and power consumption traces of IoT devices, such as smart fans and lamps, could leak personal activities in households. Our tests show that injection-induced side-channel attacks could eavesdrop on the majority of these devices from over 2 m away and through walls, with a maximum distance of 30 m for recovering intelligible headphone audio. Our case studies of audio eavesdropping in several personal, public, and work scenarios further demonstrate its security consequences in the wild¹. An example of landline phones showcases the new capability of integrating EM injection and injection-induced leakage to achieve closed-loop, context-aware eavesdropping and manipulation on private conversations. Finally, we discuss the other possible analog and digital secrets that need to be further threat-modeled under this emerging threat of injection-induced EM side channel, and analyze the possible mitigations, highlighting the urgent need for systematically examining the pervasive threat of injection-induced EM side channels. The main contributions of this work are summarized as follows:

- Theoretical framework for *Injection-Induced EM Side Channels* of analog secrets. We identify ubiquitous nonlinear hardware as the root cause of this new phenomenon, enabling future research to integrate closed-loop data eavesdropping and manipulation analysis.
- Technical design and implementation of *InjectEave*.

¹Demos and data are available at: <https://injecteave.github.io/>

Our design exemplifies how to exploit this new vulnerability, enabling through-wall eavesdropping on low-frequency analog secrets such as speech audio and activities of smart home devices, and achieving a long-range audio eavesdropping capability of up to 30 m.

- Characterization of threats and mitigation. Our evaluation on 11 COTS devices gauges this new threat model’s impact, based on which we analyze possible defense methodologies for stronger EM security protection.

2 Background

This section introduces the motivation for exploring the new techniques of injection-induced side channels, by reflecting on the history and limitations of conventional side channels and the new opportunities.

2.1 Conventional EM Side Channel

A conventional EM side channel is an unintentional one-way communication channel between the target device and an eavesdropper. Operations of computer systems are physically implemented by changing voltages (and equivalently, currents) in hardware circuits, which generate varying electromagnetic fields. Then, an electrical trace, such as a wire on the PCB or a communication cable, can act as an unintentional antenna that unwittingly sends the internal EM energy to the surrounding environment. Denoting the internal voltage signal of the secret as $V_{sec}(t)$, the side-channel leakage process can be represented as: $V_{eav}(t) = h_{lx}(V_{sec}(t))$, where $h_{lx}(t)$, with its frequency-domain representation denoted as $H_{lx}(f)$, is the transfer function describing the frequency response of the unintentional leakage source and the EM propagation path.

While adversaries trying to get higher-amplitude signals have control over H_{lx} to some degree by reducing their physical distance from the target, or employing higher-gain receiving antennas, the majority of the usable leakage signal is determined by the frequency and amplitude of $V_{sec}(t)$ itself, and the efficiency of H_{lx} over the frequency bands of $V_{sec}(t)$. For eavesdroppers, unfortunately, the efficient frequency of H_{lx} and the frequency of the interested signals $V_{sec}(t)$ often face a mismatch, as shown in Fig. 2. Taking human speech audio signals as an example, the target signals are in the range of 20 Hz–20 kHz, which is far from the feasible EM frequency range (at least on the order of MHz) of most unintentional antenna structures within the target device. Furthermore, the feasible eavesdropping distances have been limited due to the increasingly lower operation voltages of low-power miniaturized electronics [12] that reduced the amplitude of $V_{sec}(t)$, and stronger EM shielding [55] that reduced the amplitude of H_{lx} in newer computer systems.

As a result, EM side-channel leakage has so far remained a notable risk mostly for high-voltage digital data transmissions,

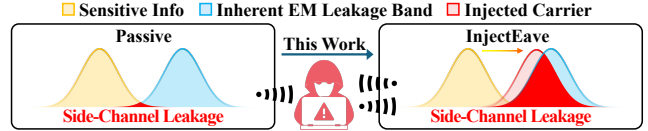


Figure 2: Injected EM carriers can piggyback secret signals, overcoming the mismatch between target signal frequencies and efficient EM emissions.

such as computer display images [33] and keyboard inputs transmitted over USB cables [73], revealing a gap in side-channel analysis capability for low-frequency analog secrets.

2.2 EM Injection and Device Nonlinearity

EM injection is a technique used to physically inject false analog signals into computer hardware. In 2013, Foo Kune et al. [35] demonstrated that amplitude-modulated EM waveforms can accurately change the analog sensor readings of implanted defibrillators and microphones. The core of EM injection methodologies is the exploitation of nonlinear hardware components for addressing the mismatch between the frequency of intended malicious signals and the effective EM injection frequency bands, which are, again, determined by the target hardware’s EM frequency response.

For example, [35] was able to inject kHz-range fake speech audio into microphone readings, where audio signals are amplitude-modulated onto EM carriers of 840 MHz. The target device’s electrical traces act as unintentional receiving antennas that pick up the modulated carriers. When the received high-frequency signals pass through microphones’ amplifiers, which have unmodeled nonlinear input-output relationships, the baseband false audio signals will be demodulated to the original frequency range and become inputs of microphones and other sensors.

Since then, EM injection has been widely considered as a means for compromising data availability and integrity, such as injecting false keystrokes [26, 85], inducing fake touchscreen inputs [47, 64], and altering camera images [24, 90]. However, our work discovers and characterizes the hidden capability of EM injection for inducing side-channel leakage and enhancing security analysis on data confidentiality: *the nonlinearity of hardware may not only demodulate information from EM carriers, but also modulate secrets onto EM carriers*. This new perspective addresses exactly the knowledge gap in the need for more effective EM side-channel methodologies that can capture low-frequency analog secrets.

3 Injection-Induced EM Side Channel

Based on the observations and analysis above, this section provides the threat model and formulation of injection-induced

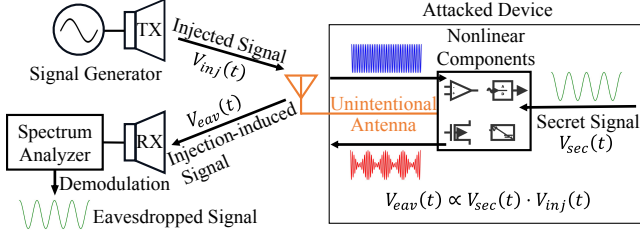


Figure 3: Model of the injection-induced leakage process.

EM side channels, and characterizes its feasibility in widely found nonlinear hardware within computer systems.

3.1 Threat Model

We hypothesize that EM signals injected into nonlinear computer hardware can mix with and thus piggyback secret information within the target system; the modulated EM signals will then leak to side-channel adversaries. In particular, the injected EM energy boosts the amount of side-channel leakage, enabling adversaries to get information previously inaccessible with conventional EM side-channel methods.

Adversary’s Objective. The objective of the adversary is the same as that in conventional EM side-channel analysis [33, 41, 73]: inferring confidential information about a computer system’s operations by analyzing the EM signals the adversary can collect. Our analysis in this work focuses on secrets in the form of analog signals, particularly the low-frequency signals such as human speech audio (below 20 kHz), power consumption and actuation control signals (below 200 Hz), which are known to be highly challenging targets due to the spectral mismatch between these secrets’ frequencies and efficient EM leakage frequencies (MHz or GHz range) [34, 79].

Adversary’s Capability. We assume the adversary has a set of readily available commercial equipment that is able to both send EM injection signals and receive modulated EM emissions. The added EM injection capability is the only difference from the assumed capability of conventional EM side-channel adversaries. The equipment often includes antennas, RF sources such as software-defined radio devices (e.g., USRP [16]), and potentially more advanced spectrum analyzers and signal generators commonly found in RF research labs. As in conventional EM side-channel research, we assume the adversary has prior knowledge of the target device’s model and can acquire a similar device for profiling its effective EM injection and emission frequencies.

3.2 Leakage Modeling

We formalize the Injection-Induced Side Channel through an *Injection-Modulation-Emission* model, as depicted in Fig. 3.

Injection Coupling. The adversary generates an injection

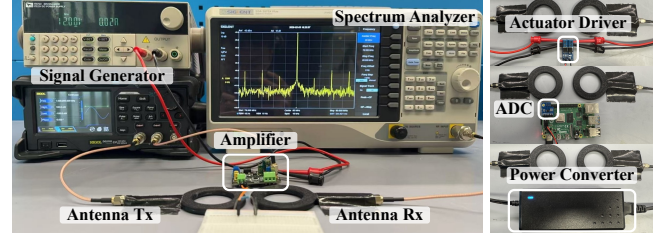


Figure 4: Feasibility tests on the most common and ubiquitous nonlinear hardware components.

carrier $V_{inj}(t)$ at frequency f_c : $V_{inj}(t) = A_{inj} \cos(2\pi f_c t)$. The target device’s electrical traces act as unintentional receiving antennas, where the injection coupling efficiency is governed by a frequency-dependent injection transfer function $H_{rx}(f)$ (equivalently, $h_{rx}(t)$ in the time domain). The induced voltage $V_c(t)$ at the input of the vulnerable nonlinear component is:

$$V_c(t) = |H_{rx}(f_c)| \cdot A_{inj} \cos(2\pi f_c t + \phi) \quad (1)$$

Consequently, the total signal $V_{in}(t)$ present at the input terminal of the nonlinear component is the superposition of the original secret signal and the coupled carrier:

$$V_{in}(t) = V_{sec}(t) + V_c(t) \quad (2)$$

Nonlinear Modulation. Following the series expansion model for semiconductor nonlinearity established in prior EMI research [35], we approximate the transfer function of the nonlinear hardware component as:

$$V_{out}(t) = \sum_{k=0}^{\infty} \alpha_k V_{in}^k(t) = \alpha_0 + \alpha_1 V_{in}(t) + \alpha_2 V_{in}^2(t) + \dots \quad (3)$$

where α_k represents the k -th order coefficient. While the linear term α_1 represents intended signal conditioning such as amplification, the quadratic term α_2 and higher-order terms induce inter-modulation. Taking the quadratic term for example, substituting Eq. (2) into the quadratic term yields:

$$\begin{aligned} \alpha_2 V_{in}^2(t) &= \alpha_2 [V_{sec}(t) + V_c(t)]^2 \\ &= \alpha_2 [V_{sec}^2(t) + V_c^2(t) + \underbrace{2V_{sec}(t)V_c(t)}_{\text{AM Modulation}}] \end{aligned} \quad (4)$$

The cross-product term in Eq. (4) exemplifies how the secret could be modulated onto the injected carrier. Denoting the aggregate signals carrying the modulated secret as $V_{sec}^c(t)$, the model shows:

$$V_{sec}^c(t) = 2\alpha_2 V_{sec}(t)V_c(t) + V_{hi}^c(t), \quad (5)$$

where $V_{hi}^c(t)$ represents the high-order inter-modulation products associated with α_3, α_4 , etc. This process effectively up-converts the spectral energy of $V_{sec}(t)$ from the baseband to the sidebands centered at f_c .

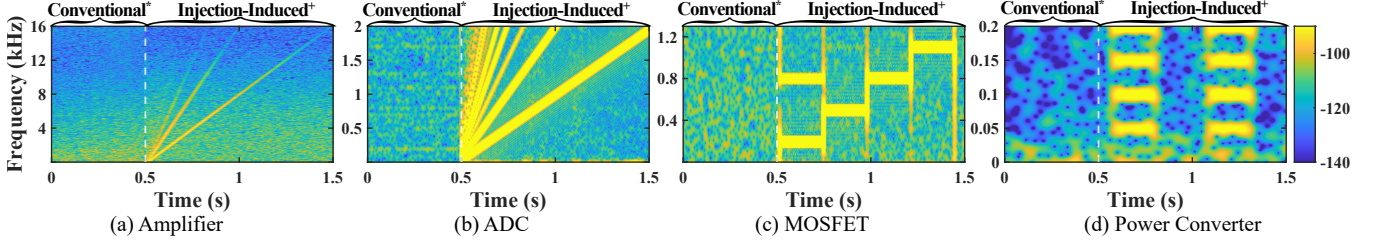


Figure 5: Ubiquitous nonlinearities in commodity computing hardware can unintentionally leak secret analog information under EM injection. *Directly measured baseband signal. +Baseband signal recovered by down-converting from the carrier frequency. The two segments of signals are concatenated together post-hoc for easier comparison.

Carrier Emission. The modulated signal $V_{sec}^c(t)$ propagates through the device’s conductive paths and emits at other electrical interconnects, which act as unintentional transmitting antennas. The leakage efficiency is determined by the emission transfer function $H_{tx}(f)$. The final leakage signal $V_{eav}(t)$ observed by the adversary is:

$$V_{eav}(t) = 2\alpha_2 \cdot h_{tx}(V_{sec}(t)V_c(t)) + h_{tx}(V_{hi}^c(t)) \quad (6)$$

When only considering the dominant second-order intermodulation for simplicity, the leakage amplitude $|V_{eav}(t)|$ can be expressed as a function of the system parameters:

$$|V_{eav}(t)| \propto \underbrace{|H_{tx}(f_c)H_{rx}(f_c)|}_{\text{Coupling Efficiency}} \cdot \underbrace{|\alpha_2|}_{\text{nonlinearity}} \cdot \underbrace{|V_{sec}(t)| \cdot |V_{inj}(t)|}_{\text{Signal Amplitude}} \quad (7)$$

The modeling reveals that even if the original secret signals’ amplitudes are low and their frequencies are significantly lower than the efficient emission frequencies of $H_{tx}(f)$, the adversary can amplify the leakage by tuning the injection frequency f_c to maximize the compound efficiency product $|H_{tx}(f_c)H_{rx}(f_c)|$, as well as by increasing the amplitude A_{inj} of EM injection $V_{inj}(t)$.

3.3 Feasibility Analysis

To verify this hypothesis of injection-induced leakage caused by inter-modulations of $V_{sec}(t)$ and $V_{inj}(t)$, we individually characterized the leakage behavior of four types of the most common nonlinear hardware found in computer systems, including (1) amplifiers, (2) analog-to-digital converters (ADCs), (3) switching Metal-Oxide-Semiconductor Field-Effect Transistors (MOSFETs), and (4) power converters. As shown by the setup in Fig. 4, we used two near-field electromagnetic probes to inject EM energy into and receive emissions from the nonlinear components.

3.3.1 Susceptibility of Common Nonlinear Electronics

For each nonlinear component, we measured the electromagnetic emissions under both conventional passive eavesdropping conditions and our proposed injection-induced condi-

tions. This comparative analysis aims to illustrate the leakage-enabling capability provided by the injection-induced side channels. We first perform wideband RF spectrum sweeps from 0 to 2 GHz across all four components under passive conditions. No discernible leakage correlated with the target secret signals is observed, indicating that low-frequency secret signals are inherently difficult to recover through passive EM emissions alone. In addition, we also measured and observed no leakage signals when the nonlinear components were replaced by linear resistance loads, confirming that hardware nonlinearity is the key for injection-induced leakage.

(1) Amplifier. Amplifiers are well-known nonlinear devices [35, 70] often found in data interfaces such as audio output and sensor input circuits. We selected Analog Devices’ AD623, a widely used rail-to-rail instrumentation amplifier, as our primary target. To characterize its nonlinear response in a controlled setting, we used a signal generator to directly input a baseband frequency sweep signal ($V_{sec}(t)$) into the amplifier’s input terminal. The sweep secret signal ranged from 0 to 16 kHz with an amplitude of 200 mV. Simultaneously, we targeted the device with an EM injection carrier $V_{inj}(t)$ at 80 MHz. The results, visualized in Fig. 5 (a), clearly show the spectral content of the original secret signal, together with distinct harmonic components ($2 \times f_{secret}$, $3 \times f_{secret}$, ...). This observation further provides proof of the hardware’s nonlinearity. In contrast, conventional eavesdropping of the 0–16 kHz analog secret shows no visible signals on the receiver.

(2) ADC. Analog-to-digital converters, another type of ubiquitous component in modern digital computer systems that process inputs of analog physical information, also have nonlinear characteristics. We used Texas Instruments’ ADS1115, a common 16-bit ADC, as the test target. Similar to the amplifier test, we input a baseband sweep signal $V_{sec}(t)$ while targeting the device with the RF carrier at 80 MHz. As shown in Fig. 5, clear secrets and their harmonic signals are observed in the injection-induced leakage, while the conventional side channel analysis receives no useful information. Notably, the results in Fig. 5 (d) reveal that leakage persists even when the injection bandwidth far exceeds the ADC’s sample rate, which is 860 Hz, revealing that modulation occurs in the continuous-time analog front-end.

(3) Switching MOSFET in Actuators. Driver circuits of actuators allow computer systems to control external hardware, such as motors in IoT devices. These circuits typically employ nonlinear power MOSFETs acting as high-speed switches to provide control signals, such as pulse width modulation (PWM). To examine their injection-induced leakage, we constructed a representative driver circuit using a discrete MOSFET driving a resistive load. An Arduino generates the baseband secret signal, $V_{sec}(t)$, in the form of a frequency-stepped square wave (shifting between 300 Hz, 600 Hz, 900 Hz, and 1200 Hz). This signal simulates a typical variable-speed motor control sequence. Simultaneously, the EM injection carrier $V_{inj}(t)$ couples onto the high-current loop formed by the Drain-Source path and the load. The recovered spectrogram shown in Fig. 5 displays a clear “staircase” pattern corresponding to the frequency steps. Nevertheless, strong harmonics accompany each fundamental frequency.

(4) Power Converter. The AC-DC rectification stage of power converters is the entry point of electrical energy for electronic devices, converting high-voltage AC mains into DC power. To investigate leakage from power supply units, we connected a power converter with a fixed high-power resistive load. Here, the target secret signal could be the AC mains voltage itself ($V_{sec}(t)$ at 50 Hz), representing the power consumption of the device. The measurement results (Fig. 5) reveal a prominent modulation effect: the fundamental mains frequency and a rich set of harmonics (e.g., 100 Hz, 150 Hz) are clearly recovered as sidebands around the carrier. This strong modulation arises from the bridge rectifier diodes at the adapter’s input. Consistently, no signal appeared in the passively eavesdropped traces.

3.3.2 Leakage Characteristics

After confirming the existence of injection-induced leakage, we further seek to characterize the quantitative relationships between the injection, leakage, and secret signals. We observe that injection-induced side channels introduce both the benefit of secret signal amplification and the challenge of nonlinear distortions.

Near-Linear Signal Amplification. We reused the setup above to produce different strengths of secret and injection signals to examine the quantitative relationship revealed by Eq. (7). Our experiments confirm the near-linear relationship between $|V_{eav}(t)|$, $|V_{sec}(t)|$, and $|V_{inj}(t)|$. For example, Fig. 6 shows the variations of these quantities on the AD623 amplifier, where $|V_{eav}(t)|$ scales almost proportionally with $|V_{sec}(t)|$ and $|V_{inj}(t)|$. Results of the other three nonlinear components exhibit highly similar trends and are thus omitted. This result thus demonstrates the capability of injection-induced EM side channels in leaking fine-grained signals, where the eavesdropped signals can vary continuously according to the original analog secrets and the intended amplification controlled by the EM injection signal.

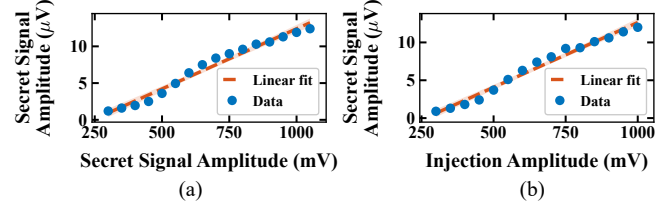


Figure 6: The amplitude of the leakage signal is jointly determined by the strength of the secret and injection signals.

Challenge of Nonlinear Distortions. Although the linear amplification effect of the second-term inter-modulation provides injection-induced side channels with the unique capability of controllable leakage strength, it also inevitably faces the distortions caused by the higher-order terms ($V_{hi}^c(t)$ in Eq. (5)). This is illustrated by the nonlinear variations of the data points in Fig. 6, and could manifest as harmonics of the original secret signal (e.g., as shown in Fig. 5). While the harmonics are discernible when the secret is a simple single tone, they may degrade the quality of more complex wideband signals by contaminating the original frequency components. For example, human speech signals naturally consist of a fundamental component and its harmonics, meaning that higher-order inter-modulation products of the fundamental and even lower-order harmonics can overlap with, and thereby distort, higher-frequency components, posing a unique challenge for reconstructing high-quality audio and other wideband secrets.

3.4 InjectEave Design

Based on the new knowledge about the capability and challenge of injection-induced side channels, we provide an exemplary eavesdropping design, named InjectEave.

EM Injection and Receiving Hardware. Aiming for a portable and efficient design, InjectEave uses an Ettus USRP B210 and a Log-Periodic antenna to send single-tone injection signals at its maximum output power. On the leakage receiver side, another Log-Periodic antenna connected to a Siglent SSA3075X Plus spectrum analyzer collects the leaked electromagnetic signals. The spectrum analyzer demodulates the signal at the same center frequency as the USRP’s output. The resulting baseband signal is routed to a recording device, such as a laptop, for further processing. The hardware setup is shown in Fig. 7.

Frequency Profiling. To identify effective injection carriers, we use a two-stage coarse-to-fine frequency profiling procedure. During this process, target devices are set to their typical operating states: audio devices continuously play a 2 kHz single-tone signal, smart fans operate at maximum speed, and smart lamps are profiled using the 50 Hz power-frequency component. We first conduct a coarse-grained frequency sweep from 70 MHz to 2 GHz with a 10 MHz step size to locate effective frequency ranges. Subsequently, a

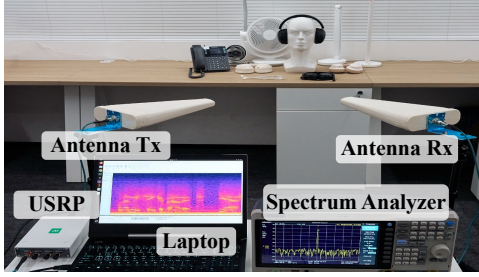


Figure 7: The hardware setup for evaluating COTS devices.

fine-grained frequency sweeping is performed within these effective ranges using a 1 MHz step. By comparing the leakage strength across all frequency candidates, we select the one with the highest leakage strength as the optimal carrier.

Signal Enhancement Software. To address the observed distortions, especially for audio signal eavesdropping, we employ a Score-based Generative Model for Speech Enhancement (SGMSE) [78] backend and treat the noisy measurement as a structural anchor.

The reconstruction is formulated as a mean-reverting diffusion process driven by two distinct mechanisms. The drift term uses the leakage as a structural constraint, locking the generation to the envelope $|V_{eav}(t)|$ to preserve the victim’s original prosody. Simultaneously, the score function acts as a spectral enhancer, specifically filtering out the inter-modulation distortions $V_{hi}^c(t)$ to restore high-fidelity speech.

The effectiveness of the model relies on training with a large-scale synthesized dataset of paired clean and distorted signals. Given the practical difficulty of collecting aligned EM data in the wild, the speech enhancement model is trained solely on synthesized data, with training pairs generated using a physics-based pipeline derived from Eq. (5). We use LibriSpeech [56] as the clean speech dataset and synthesize the corresponding leakage traces by applying various device-agnostic nonlinear coefficients to simulate the hardware non-linearity of possible devices, combined with ambient EM noise. Since physical devices differ in their nonlinear coefficients, the trained model is evaluated on unseen devices to assess its cross-device generalizability. This approach ensures the model learns the unique spectral structure of these inter-modulation distortions $V_{hi}^c(t)$, enabling robust generalization to real-world hardware leakage. As demonstrated in ??, enhanced audio exhibits significant improvements in both standard audio quality metrics and intelligibility. The audio demos can be found in [6].

4 Evaluation in a Laboratory Setting

This section evaluates `InjectEave` attack on 11 commercial devices of 5 different categories and measures the eavesdropping attack’s performance in real-world settings.

4.1 Experimental Setup

Fig. 7 shows the laboratory setup. The adversary’s equipment consists of a USRP, directional Tx/Rx antennas, a spectrum analyzer, and a laptop. The laptop controls the USRP to generate the injected carrier, which is transmitted through the Tx antenna toward the target device. The Rx antenna captures the injection-induced EM leakage from the target, and the received signal is observed and measured by the spectrum analyzer. The evaluated COTS devices are placed on the desk as victim devices during the experiment.

Victim Devices. The evaluated devices included: (1) three wired headphones from Sony, Dell, and Apple; (2) three wireless headphones from UGreen, PHILIPS, and HP; (3) a wireless landline from Flyingvoice; (4) two smart fans from Xiaomi and OIDIRE; and (5) two smart lamps from Xiaomi and JINGZAO. The detailed information of each device is specified in Table 1.

Metrics. We evaluate the overall performance of `InjectEave` attack on the signal, feature, and semantic levels respectively, using two primary metrics:

(1) *Signal-to-Noise Ratio (SNR)* characterizes the signal-level quality of the injection-induced EM leakage and the recovered signal at specific distances. (2) *Attack Success Rate (ASR)* provides a unified measure of recovered information fidelity relative to the ground truth. For audio devices, ASR is defined as $1 - WER$, where word error rate (WER) evaluates the accuracy of recovering a speech signal’s semantic information. We compute WER by first transcribing the recovered speech using Whisper [59], and comparing the transcript with the ground-truth script at the word level, where substituted, missing, and extra words are counted as errors. For discrete-state devices, including smart fans and smart lamps, ASR is defined as the classification accuracy ($N_{correct}/N_{total}$) across all operational states.

4.2 Evaluations on COTS Devices

We categorize the analysis on the 11 COTS devices into two distinct threat dimensions based on the attack surfaces and exposed privacy risks: high-fidelity audio recovery and human activity inference. Specifically, audio peripherals serve as direct attack vectors for speech eavesdropping. In contrast, smart home devices’ states can be exploited to infer user presence and behavioral patterns.

To systematically evaluate the attack performance, we first conduct measurements at 50 cm across all devices, quantifying the injection frequency, SNR, and signal recognition rate, before further evaluating the maximum achievable attack distance. Table 1 reports the SNR and recognition rate at 50 cm. We establish a device-specific SNR threshold from 30 trials, set to the lowest observed SNR, and then conduct another 30 independent trials, counting a trial as successful if the measured leakage SNR exceeds this threshold. For maximum

Table 1: Summary of Attacks on COTS Devices

Device Type	Brand	Model	Year	Source of leakage	Injection Frequency	SNR ‡	Recog. Rate §	Max Dist. ¶
Wired Headphones	Sony + Dell	ZX110AP	2014	Amplifier	*1*_*7* MHz	21.7 ± 0.8 dB	30/30	5 m
	Sony + Mac	ZX110AP	2014		*2*_*6* MHz	13.9 ± 0.6 dB	30/30	4 m
	Apple + iPhone	Earbuds	2016		*6*_*8* MHz	5.9 ± 0.5 dB	29/30	1 m
Wireless Headphones	UGreen [†]	MAX2	2024	Amplifier	*0*_*8* MHz	23.1 ± 0.7 dB	30/30	6 m
	PHILIPS	TAH2020	2025		*9*_*5* MHz	20.9 ± 0.7 dB	30/30	6 m
	HP	H231R	2023		*8*_*2* MHz	19.9 ± 0.8 dB	29/30	4 m
Landline	Flyingvoice	P23GW	2023	ADC & Amplifier	*4*_*2* MHz	12.9 ± 0.6 dB	30/30	3 m
Fan	OIDIRE [†]	ODI-MF10A	2023	Switching MOSFET	*4*_*2* MHz	38.6 ± 0.5 dB	30/30	6 m
	Xiaomi	BPLDS10DM	2025		*3*_*1* MHz	30.0 ± 0.5 dB	30/30	4 m
Lamp	JINGZAO	JDO-06	2024	Power Converter	*8*_*5* MHz	20.0 ± 0.7 dB	29/30	3 m
	Xiaomi [†]	1S	2019		*7*_*0* MHz	21.6 ± 0.8 dB	30/30	3 m

||: Three different host devices for wired headphones. *: We intentionally hide the injection frequency for ethical considerations. †: Devices evaluated in Section 4.3. ‡: SNR is evaluated at 50 cm distance and reported as mean ± standard deviation across 30 independent trials. §: Recognition rate is evaluated at 50 cm distance. ¶: Max distance is evaluated at 5/30 recognition rate.

distance evaluation, the detection SNR threshold is defined as $10\log_{10}(10/B_n)$, derived from a noise-only spectrum with a 10 Hz resolution bandwidth, where B_n is the observation bandwidth. For audio devices (wired headphones, wireless headphones, and landlines), we set $B_n = 20$ kHz to cover the audible speech band; for fans and lamps, $B_n = 150$ Hz, covering three times the leakage frequency. These bandwidths yield detection thresholds of -33.0 dB for audio devices and -11.8 dB for fans and lamps.

4.2.1 Threats Against Audio Peripherals

Audio peripherals, including wireless headphones, wired headphones, and landlines, are ubiquitous in both public and private spaces. To evaluate `InjectEave` attack on these COTS audio peripherals, we play a 2 kHz reference single-tone signal, which represents a typical speech signal frequency, on the devices. As shown in Table 1, `InjectEave` achieves a near 100% signal recognition rate across these devices, with each device exhibiting injection-sensitive frequency ranges that allow flexible carrier selection.

Wired Headphone. We evaluate `InjectEave` attack on wired headphones to demonstrate effectiveness across different host-device interfaces. As summarized in Table 1, we achieve a near 100% recognition rate at 50 cm across all setups. The optimal injection frequency for the Sony ZX110AP exhibits a significant host-dependent shift, requiring a distinct frequency band when connected with the MacBook Pro M2 compared to the Dell G5.

Despite these variations, the attack remains robust with effective ranges of 5 m and 4 m, respectively. In contrast, the Apple Earbuds on an iPhone 15 Pro achieves an SNR of 5.9 dB and a 1 m range. These results indicate that the

analog amplifier of the host device’s internal sound card is the fundamental component exploited for injection-induced EM leakage, while the headphone cable primarily acts as an unintentional antenna. The distinct grounding and circuit layouts of the Dell and MacBook sound cards determine the specific resonant frequencies required for inter-modulation, resulting in the phenomenon that the same headphone is susceptible at different injection frequency bands.

Wireless Headphone. We evaluate three wireless models, each exhibiting high susceptibility to `InjectEave` across distinct frequency bands as detailed in Table 1. The UGreen MAX2 demonstrates the most robust leakage, achieving an SNR of 23.1 dB and a 100% recognition rate with an effective distance of up to 6 m. Similarly, the PHILIPS TAH2020 supports a 100% recognition rate with an SNR of 20.9 dB and a 6 m range. Even the HP H231R maintains a 29/30 recognition rate and a 4 m distance. We further validate the real-world threat of `InjectEave` in Section 5.1, where we achieve successful through-wall audio eavesdropping in real-world hotel and conference room scenarios.

Landline. Landline desk phones are often used in high-sensitivity scenarios such as government offices for internal communications [31]. To examine risks in these professional environments, we extend our evaluation to a Flyingvoice P23GW VoIP landline. We simulate an active call and sweep the carrier frequency to locate sensitive nonlinear junctions within the handset’s internal amplifier and ADC stages. As summarized in Table 1, the system exhibits high susceptibility, achieving a 100% recognition rate and an SNR of 12.9 dB. The attack remains viable at distances up to 3 m, allowing an adversary to eavesdrop on confidential corporate negotiations without compromising the digital network. We further

demonstrate the severity of this threat in Section 5.2, where InjectEave is used to achieve closed-loop manipulation of the landline’s voice interface.

Effect of Audio Signal Enhancement. We further examine the effectiveness of the eavesdropping design in Section 3.4 on 2 minutes of speech audio recordings captured at a distance of 50 cm with 65 dB volume from the UGreen MAX2 wireless headphone using both SNR and Short-Time Objective Intelligibility (STOI), a standard speech quality metric. The results show notable improvements in both STOI and SNR. The average SNR increases drastically from 7.0 dB to 16.1 dB, indicating that the model successfully suppressed the dominant background noise and the injection-induced carrier phase noise. Furthermore, STOI sees a significant boost from 0.58 to 0.72. Given that STOI is highly correlated with human speech intelligibility, this improvement confirms that our algorithm effectively reconstructs the phonetic details masked by the hardware’s nonlinear harmonics, rendering the eavesdropped speech intelligible to human listeners. Our demos can be found in [6].

Cross-device Profiling Transferability. We evaluate cross-device profiling transferability using three UGreen MAX2 headphones of the same model. For each headphone, we profile its effective carrier frequency and directly reuse it to attack the other two without re-profiling. All cross-device profiling attacks succeed in our experiments. The transferred attacks achieve leakage SNRs of 23.2–24.6 dB, with only 0.8–2.9% relative deviation compared with attacks using device-specific profiling. This good profile transferability mainly stems from the fact that the profiled frequency (942 MHz) is identical across three devices and also indicates that the effectiveness of transferability is largely determined by the shared analog front-end layout, cabling structure of the same model, rather than by batch or manufacturing differences.

4.2.2 Threats Against Smart Home Appliances

Beyond audio-centric devices, we examine the generalizability of the attack on IoT smart appliances, which are deeply integrated into private environments. The main leakage source shifts from audio amplifiers to the switching MOSFETs in fans and power converters in lamps.

Smart Fan. The OIDIRE ODI-MF10A and Xiaomi BPLDS10DM smart fans feature operational modes—such as Sleep, Natural, and Standard—that serve as proxies for the user’s activity. The attack exploits the modulation caused by the motor’s driving signal, where the rotational speed (e.g., low: 27 Hz, medium: 40 Hz, high: 50 Hz) modulates the injected carrier. As shown in Table 1, the OIDIRE model yielded an SNR of 38.6 dB at 480 MHz, maintaining a successful recognition rate up to 6 m. Unlike audio devices, the fan’s leakage manifests as sidebands at distinct frequency offsets in the frequency domain (Fig. 8 (a)). This enables “Context Inference” attacks: for example, detecting “Sleep

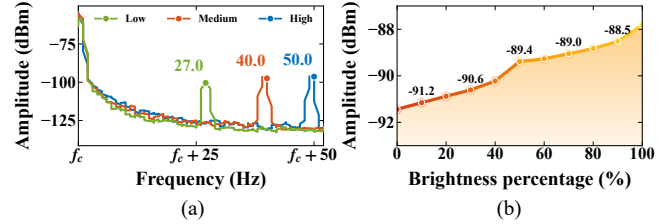


Figure 8: Eavesdropping on smart home activities: (a) inferring fan speed, and (b) inferring lamp brightness.

Mode” at night can confirm a user’s rest schedule and infer occupancy without the need for visual surveillance.

Smart Lamp. We further tested the Xiaomi 1S and JD JINGZAO JDO-06 smart lamps. The mechanism exploits the nonlinearity of the lamp’s power converter, where the 50 Hz AC mains current modulates the injected carrier. As indicated in Table 1, the Xiaomi 1S exhibited strong leakage with an SNR of 21.6 dB. Since the amplitude of the demodulated signal is proportional to the power load, we can remotely infer the precise dimming level. By mapping these power levels to vendor-specific presets (e.g., 20% brightness for “Reading”), an adversary can perform “Behavioral Profiling,” transforming a simple light source into a beacon that exposes a user’s specific activities and routines without requiring any network-level access. Fig. 8 (b) demonstrates how adversaries could precisely infer the lamp’s brightness from the strength of received signals, effectively enabling power side-channel analysis [10, 50] in a contactless manner.

4.3 Environmental Impact Quantification

To characterize the physical limits and practical constraints of InjectEave attack, we select three representative devices for impact quantification: the UGreen MAX2 wireless headphones, the OIDIRE ODI-MF10A smart fan, and the Xiaomi 1S smart lamp. Unless otherwise specified, our default experimental configuration employs a 50 cm attack distance, a 90° antenna orientation, and an injection power of 18 dBm. The carrier frequencies are configured at 940 MHz, 480 MHz, and 100 MHz for wireless headphones, smart fan, and smart lamp, respectively, corresponding to their optimal resonant points discovered during the frequency sweep experiment. We quantify the attack robustness by varying the attack distance to determine the effective range, adjusting the antenna orientation to analyze polarization sensitivity, and introducing various material barriers to evaluate signal penetration and eavesdropping in realistic environments.

Impact of Antenna-Target Distance. To evaluate the effective eavesdropping distance and the limits imposed by propagation path loss, we varied the distance between the adversary and the victim device up to 5 m. As shown in Fig. 9 (a), the leakage SNR decreases monotonically with distance, dropping by approximately 45 dB across all devices from 10 cm

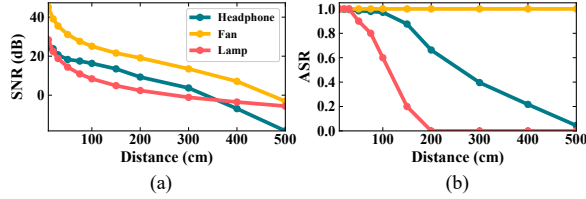


Figure 9: Impact of attack distance on (a) SNR trend and (b) Attack Success Rate (ASR) across different COTS devices.

to 5 m. The corresponding ASR results in Fig. 9 (b) reveal distinct hardware-level resilience: while the Xiaomi 1S smart lamp becomes resilient beyond 2 m and the UGreen MAX2 drops to a 4.4% ASR at 5 m, the OIDIRE smart fan maintains a 100% ASR. The attack distance can be further extended by increasing transmitting power or lowering the phase noise by using high-performance attack equipment. Replacing the Siglent SSA3075X Plus (phase noise: -98 dBc/Hz) with a high-end Keysight N9000B spectrum analyzer (phase noise: -110 dBc/Hz), which offers a superior phase noise of -110 dBc/Hz at a 1 GHz carrier with 10 kHz offset, extends the effective distance to over 8 m for UGreen wireless headphone, 10 m for OIDIRE smart fan, and 5 m for Xiaomi smart lamp. These findings highlight that *InjectEave* poses a significant long-range threat in practical environments by eliminating the requirement for physical proximity. We provide three case studies in Section 5 to show the real-world threat of *InjectEave* attack in the wild.

Impact of Antenna Angle. To investigate the impact of the relative angle between the transmitting and receiving antennas, we rotated the receiving antenna along the target’s azimuthal plane from 0° to 315° in 45° increments while keeping the transmitting antennas fixed. As shown in Fig. 10 (a), the leakage exhibits strong directionality, with all devices peaking at 90° . At this optimal orientation, the SNR reaches 18.3 dB, 31.1 dB, and 14.4 dB for the headphone, fan, and lamp, respectively. This phenomenon occurs because a 90° spatial separation maximizes isolation between the antennas, effectively suppressing direct carrier leakage into the receiver. This prevents receiver saturation and lowers the noise floor, thereby maximizing the SNR of the recovered side-channel signal. The ASR in Fig. 10 (b) largely follows the SNR trends but reveals a task-specific resilience. For the UGreen headset, the audio eavesdropping ASR fluctuates, peaking at 93.7% (90°) from a low of 50.5% (0°). We observe that attack performance is maximized when aligning the receiving antenna near the 90° orientation, providing insightful guidance for practical attack design and deployment. Nevertheless, precise alignment to 90° is not strictly required in practice, as the recognition rate remains above 86% even with a 15° deviation from the optimal 90° orientation.

In contrast, state-based inference is remarkably robust: the OIDIRE smart fan maintains a consistent 100% ASR in all

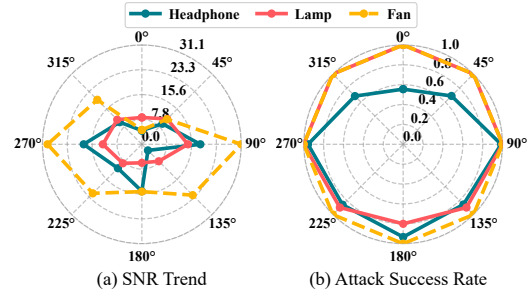


Figure 10: *InjectEave*’s robustness against antenna angles. The results indicate optimal performance at 90° .

orientations, while the Xiaomi smart lamp sustains a high ASR with only minor fluctuations between 135° and 225° .

Impact of Physical Barrier. To evaluate *InjectEave* in non-line-of-sight (NLoS) environments, we measured the signal attenuation caused by common structural materials, including glass, wood, and concrete. As shown in Fig. 12 (b), these barriers exert minimal influence on the leakage SNR. Glass and wood induce a negligible attenuation of only 1–2 dB compared to line-of-sight (LoS) conditions. Concrete obstacles cause a more pronounced but still limited drop: 5.8 dB for the headphone, and approximately 2.5 dB for the fan and lamp. The ASR remains remarkably resilient across all tested materials in Fig. 12 (c). For glass and wood, the ASR remains unchanged for all devices. Even with concrete, the impact is marginal: the headphone ASR decreases by only 3%, while the smart fan maintains a 100% success rate. These results demonstrate that *InjectEave* effectively penetrates common structural barriers, enabling covert through-wall eavesdropping in partitioned indoor environments such as offices and hotels, as further detailed in Section 5.

5 Audio Eavesdropping in the Wild

This section moves beyond controlled laboratory characterization to demonstrate end-to-end audio eavesdropping in realistic environments. Our case studies in Fig. 11 focus on non-line-of-sight (NLoS) scenarios where the adversary is physically separated from the victim and performs through-wall attacks against victim-side audio devices. By launching *InjectEave*, the adversary can recover a remote participant’s voice without physical access to the speaker. We further examine practical deployment factors, including playback volume, nearby active electronics, ambient RF interference, and injection stealthiness. Finally, we demonstrate two extended threats: a closed-loop attack that synthesizes and injects recovered speech back into the victim device, and longer-distance eavesdropping enabled by an external power amplifier.

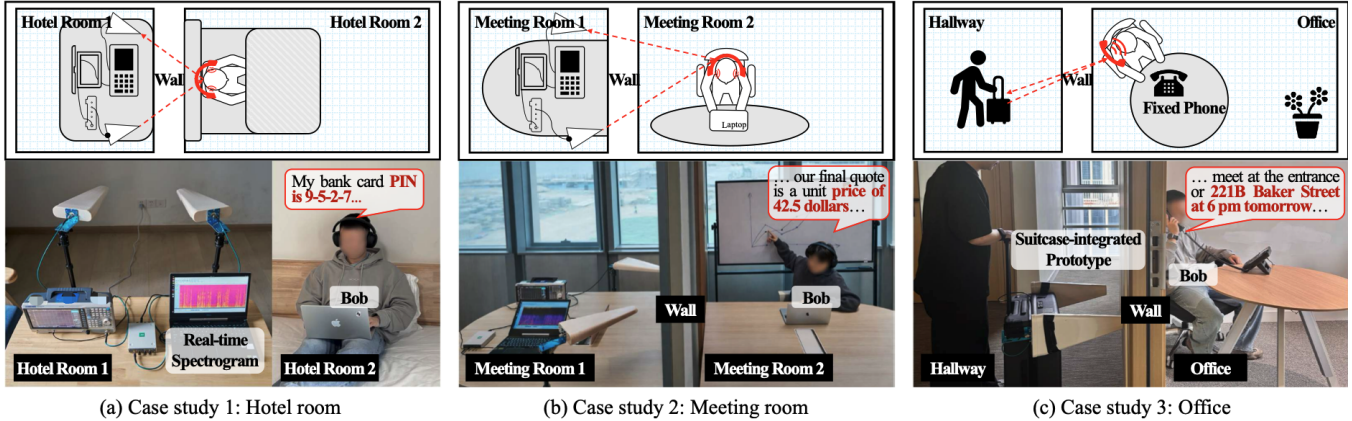


Figure 11: Case studies of representative audio eavesdropping scenarios in the wild.

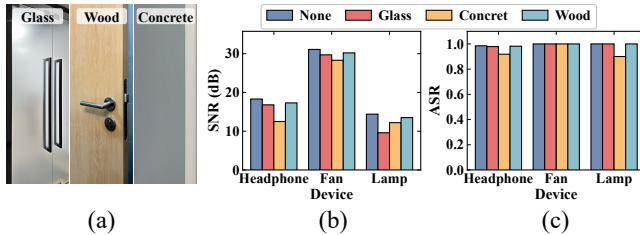


Figure 12: Impact of different barriers on InjectEave performance, showing feasibility of through-wall eavesdropping in real-world non-line-of-sight (NLoS) environments.

5.1 Real-World Audio Eavesdropping

This case study demonstrates that the injection-induced side channel can be exploited to conduct through-wall eavesdropping to compromise individual privacy (e.g., bank PINs, personal agendas) and corporate confidentiality (e.g., procurement quotes, strategic timelines). As shown in Fig. 11 (a) and (b), we conduct end-to-end attacks in both a hotel room and a meeting room setting. In these scenarios, the victim Bob engages in a confidential video call using a UGreen MAX2 wireless headset. The adversary operates from an adjacent room, separated by a 30 cm solid concrete wall, with a straight-line distance of over 1 m. We use a commercial open-source text-to-speech (TTS) tool [1] to synthesize six personal conversation segments in both male and female voices, covering personal and business-oriented dialogues. The content of the conversation segments is provided in [6].

Fig. 13 shows a representative time-frequency analysis of the eavesdropped audio, successfully recovering a speech segment of the victim’s detailed personal agenda: “Let’s meet at the entrance of 221B Baker Street at 6 PM tomorrow.” The top panel displays the clean ground-truth audio for reference. Despite the significant attenuation caused by the solid concrete wall, the eavesdropped spectrogram (middle panel) clearly retains the fundamental harmonic structures of the

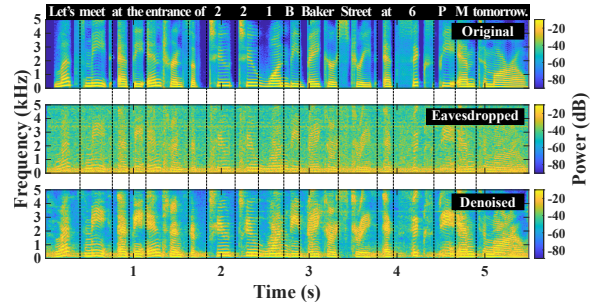


Figure 13: Comparison of audio spectrograms across the original, eavesdropped and denoised audio, demonstrating the eavesdropping performance and signal enhancement effect in InjectEave attack.

original speech. Applying the signal enhancement algorithm described in Section 3.4 significantly sharpens spectral harmonics while suppressing background interference (bottom panel). These results demonstrate that the injection-induced EM side channel enables reliable eavesdropping of Alice’s intelligible speech even through dense physical barriers, posing direct threats to private conversations.

To further evaluate the robustness of InjectEave attacks across diverse real-world teleconferencing conditions, we examine three factors that may affect attack performance: the headphone playback volume, interference from nearby active electronics and ambient RF noise, and the perceptibility of the injected carrier at the victim device.

Evaluation of Headphone’s Playback Volume. We adjust the headphone’s playback volume from a quiet office level of 60 dB to a louder entertainment level of 80 dB. As shown in Fig. 14, the SNR of the eavesdropped leakage exhibits a strong positive correlation with the playback volume. Crucially, even at a modest sound pressure level (SPL) of 65 dB, a typical threshold for private business conversations [57], the proposed InjectEave attack remains highly effective.

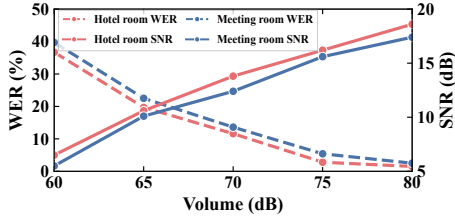


Figure 14: Impact of audio volume on SNR and word error rate of eavesdropped speech signals.

Specifically, the adversary can successfully recover Alice’s managerial instructions with an SNR of approximately 10 dB and a corresponding word error rate (WER) of roughly 22%. These metrics indicate that even at lower volumes, the attack retains sufficient phonetic information to reconstruct Alice’s intelligible speech.

Evaluation of Multi-device and Ambient RF Interference Effects. To evaluate whether *InjectEave* remains effective in a realistic environment with multiple nearby nonlinear devices and ambient RF activity, we conduct an experiment in a meeting room with diverse electronic devices, including ceiling cameras, ceiling microphone arrays, and a central air conditioner. The attack is launched on a commercial headphone while multiple nearby electronic devices operate simultaneously, including audio devices, microphones, and common household and office appliances. These devices are wirelessly connected via BLE and WiFi, representing a noisy RF environment. We measure the SNR at a 50 cm distance with the interference devices turned on versus off, and observe a deviation of only 2.2 dB, indicating that the attack remains stable in the presence of nearby active electronics and ambient RF activity. A photo and full device details are provided in Fig. 15.

This robustness against interference from nearby devices is further explained by the frequency and spatial selectivity of *InjectEave*, as demonstrated on our website [6]. Devices of different models often exhibit distinct effective frequencies, allowing the adversary to tune the injected carrier toward the target device while avoiding comparable responses from nearby non-target devices. When frequency profiles overlap for devices of the same model, antenna realignment provides spatial selectivity and keeps the target leakage dominant.

Evaluation of Injection Perceptibility. The injected carrier may induce additional voltage variations in the target circuit. To assess whether this injected energy will cause humanly detectable artifacts in the output audio, we specifically place the transmitting antenna adjacent to the target UGreen MAX2 headphone and inject the single-tone carrier at 18 dBm power, representing a worst-case scenario with large injected energy, while ensuring this setting can induce recoverable leakage. During the test, the headphone plays normal audio, and we use an external microphone to directly record the audio output from the headphone under two conditions: with



Figure 15: An office eavesdropping setting with diverse interference from multiple ceiling-mounted and desktop electronics. The injection-induced leakage remains robust to interference.

and without the injected carrier. The STOI deviation ranges from 0.001 to 0.012, with an average of 0.008. Demos [6] also show no perceptible difference in the headphone output, suggesting that the single-tone carrier does not introduce noticeable audible artifacts or distort the victim’s received audio even under aggressive near-field injection. The stealthiness is preserved because single-frequency carriers are filtered by analog front-ends, introducing little perceptible distortion.

5.2 Closed-Loop Conversation Manipulation

This case study demonstrates the real-world threat of *InjectEave* attack against critical office landline infrastructure, specifically focusing on the Flyingvoice P23GW VoIP landline phone in a private office environment. Beyond passive eavesdropping, *InjectEave* enables a novel “Eavesdrop-Synthesize-Inject” closed-loop manipulation chain that elevates the threat from compromising conversation confidentiality to falsifying speech content. As shown in Fig. 11 (c), the victim, Bob, is at his desk and engaged in a call with his boss, Alice. The adversary packs the portable attack hardware into a suitcase-based prototype and stands in the hallway, maintaining a standoff distance of 50 cm from the target device, with a 20 cm office wall separating them. The internal structure of this prototype is illustrated in Fig. 17. The specific three steps for carrying out the closed-loop conversation manipulation are described as follows.

Step 1: Eavesdrop. The attack starts by eavesdropping on the conversation through the injection-induced side channel to achieve context awareness. By eavesdropping on Alice’s voice from the landline’s speaker at 880 MHz, the adversary’s system achieves a real-time understanding of the call.

Step 2: Synthesize. Alice’s recovered speech from the eavesdropping stage serves as the speaker reference for the voice-cloning module. Upon detecting predefined trigger keywords (e.g., “quote” or “confirmation”), the system activates a voice-cloning module, IndexTTS-2 [89] to generate a contextually appropriate and identity-specific deepfake response in real time. To preserve stealthiness, the adversary adjusts

the synthesized speech using the eavesdropped audio as a reference, matching Alice’s call audio in speech quality and perceived volume before modulation.

Step 3: Inject. The injected speech is amplitude-modulated onto a 1075 MHz carrier and transmitted at 40 dBm using well-established EM signal injection techniques [35, 69] through a separately profiled EM injection channel. The carrier then couples into the landline’s analog audio output path and is demodulated by the nonlinear front-end into audible speech at Bob’s headset. To avoid overlap between injected and received voice signals, Step 1 and Step 3 are designed to be time-divided: the adversary stops eavesdropping and switches to speech injection, injecting the synthesized Alice’s audio into the target landline’s audio output to complete the closed-loop manipulation. We conduct a series of trials across diverse semantic contexts to demonstrate the real-world attack impact of this closed-loop manipulation, with demos provided on our project website [6].

To quantify the perceptibility of the injected audio manipulation, we record the victim-side audio using an external microphone. Specifically, under the same recording setup, we compare Alice’s original speech directly played through Bob’s headset with the corresponding audio injected into Bob’s headset. The resulting STOI deviation is only 0.071 on average, indicating that the injected audio remains highly similar to the original speech of Alice as actually heard by Bob. Further demos can be found on [6].

5.3 Long Distance Eavesdropping

Attack distance directly affects the practical risk of InjectEave, as it determines whether an attacker can recover the victim’s low-frequency secret without close physical proximity. Based on the leakage model in Eq. (7) and the theory of signal attenuation in free space [68], we derive the theoretical maximum eavesdropping distance as: $d_{max} \propto \sqrt{|V_{inj}| \cdot |V_{sec}| / N_{sys}}$, where V_{inj} denotes the voltage amplitude of the injected carrier, indicating that the range can be extended through higher transmission power, such as utilizing amplifiers.

In our extended-range experiment for UGreen MAX2 and PHILIPS TAH2020, we increase the injection power from the default 18 dBm to 40 dBm using an external power amplifier (G41P40S) purchased from Alibaba at a cost of \$415. With this higher-power setup, InjectEave can recover audible speech information at distances up to 30 m, extending the attack range beyond the default 6 m setting. The long-distance setup with the power amplifier is shown in Fig. 16. We provide the long-range demos on our project website [6].

6 Discussion

The scope of this work is to provide the theoretical framework and exemplary designs of injection-induced EM side channels, laying the foundation for the scientific characterization of

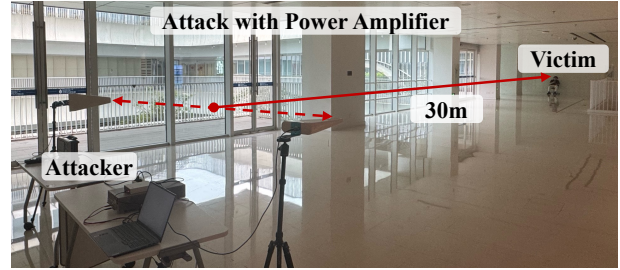


Figure 16: Long-distance eavesdropping setup with external power amplification, showing extended attack ranges of up to 30 m under higher EM injection power.

these emerging threats. Based on this framework, this section discusses the need for follow-up research, including exploring other susceptible interfaces and effective protections.

6.1 Limitations and Future Work

Attack Surface Generalizability. While our evaluation focused on common audio output devices and smart home applications as motivating and representative examples that carry low-frequency analog secrets, the fundamental leakage models prompt us to extrapolate that InjectEave represents a more generalized attack surface. Theoretically, the vulnerability of injection-induced EM side channels is inherent to any electronic system featuring unshielded nonlinear analog interfaces. We believe future work can contribute to this emerging research topic by examining the susceptibility of a broader class of targets, such as electrical communication signals internal to computer systems, and even confidential data of analog sensor inputs. Below, we discuss our preliminary analysis of audio signals of microphone inputs.

Investigation of Analog Microphone Inputs. Our exploration of analog input devices was motivated by an observation in the closed-loop attack on the landline phone in Section 5.2: we found that it was also feasible to reconstruct audio from the landline’s microphone that captures local user’s speech. Then, we further analyzed InjectEave attack on two additional commercial microphones: the UGreen CM769 and the Razer SEIREN V3 MINI. While we can successfully reconstruct intelligible audio from both devices, our experiment revealed a significantly constrained effective distance compared to the range achieved with headphone audio output. Even under ideal conditions where the target microphones were operating at maximum gain, the maximum range for audio eavesdropping is limited to approximately 30 cm. Our analysis shows that this performance disparity is rooted in the amplitude difference between the audio input and output signals. While headphone drivers typically require 1–2 V to operate, microphones generate extremely weak 1–10 mV signals. According to Eq. (5), this 40–60 dB voltage deficit results in a substantially weaker leakage signal, causing the



Figure 17: The portable prototype is integrated into a suitcase. Key components include an antenna array, an SDR transceiver, a spectrum analyzer, a laptop, and a portable power supply.

secret information to be easily obscured by the noise floor even with injection-induced leakage.

Nevertheless, this current boundary is determined by our EM injection and receiving hardware rather than an intrinsic physical limit. The theoretical maximum eavesdropping distance is $d_{max} \propto \sqrt{|V_{inj}| \cdot |V_{sec}| / N_{sys}}$, as illustrated in Section 5.3, where N_{sys} denotes the aggregate system noise floor. This shows that the range constraint can be mitigated through further hardware upgrades, such as utilizing high-gain antennas to boost $|V_{inj}|$ and using low-noise spectrum analyzers to suppress N_{sys} . We believe this can be achieved by collaborating with resourceful RF researchers as a future work.

6.2 Mitigation

We provide insights into potential hardware and software mitigations gleaned from our investigations.

Protective Coding Against EM Leakage. Existing defenses for mitigating conventional EM side-channel eavesdropping attacks, such as cryptographic masking [11] and randomized clocking [41, 54], are specifically tailored to obfuscate digital logic transitions. Thus, they are mostly ineffective against `InjectEave` as it eavesdrops on signals in the analog data interfaces. Unlike digital data, these continuous analog waveforms cannot be mathematically masked or randomized without irreversibly degrading the signal fidelity and functional integrity of the device. As a result, we believe more in-depth research is needed to investigate the design space of analog data protection and evaluate utility-security tradeoffs in mitigating emerging analog side-channel leakage.

Physical Hardening Against EM Injection. Traditional EM injection defense typically relies on electromagnetic compatibility (EMC) hardening, such as Faraday shielding [24, 28], low-pass filtering [35], and differential signaling [5, 77]. While these methods can attenuate coupling, they do not guarantee absolute security. According to Section 5.3, a well-resourced adversary can successfully conduct attacks by increasing the injection power. Furthermore, standard low-pass filters often degrade at high frequencies due to parasitic

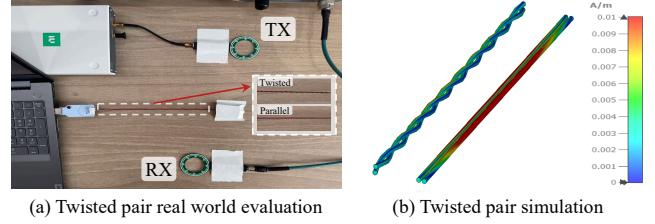


Figure 18: Evaluation of twisted-pair mitigation in real-world experiments and simulation.

inductance [67], and specialized high-end filters are rarely viable for consumer electronics. Consequently, a robust defense paradigm shifts toward active detection and mitigation. Promising approaches include monitoring for anomalous RF carriers [2] or DC offsets induced by nonlinear rectification [82], alongside software-level consistency checks via sensor fusion [71] and encoding [86]. However, implementing these protections on commercial systems requires addressing significant overheads in manufacturing costs, power consumption, and form factors.

Twisted Pair. We disassemble several devices in Table 1 to understand why some devices exhibit shorter eavesdropping ranges. Our teardown analysis reveals that devices using twisted-pair cables exhibited significantly greater resistance to the attack than those with standard parallel wires. To verify this, we build a minimal proof-of-concept setup in Fig. 18 (a), evaluating the same USB speaker at 900 MHz with either a standard parallel or a twisted-pair connection, while keeping all other parameters unchanged. The speaker continuously plays a 2 kHz single-tone signal. Under the parallel-pair configuration, the measured injection-induced leakage SNR is 37.6 dB, which decreases to 26.9 dB after switching to twisted-pair wiring, corresponding to a 10.7 dB reduction. To further quantify this effect under ideal conditions, we perform a CST full-wave simulation on a parallel pair with 1.2 mm spacing and an equivalent twisted-pair geometry under identical 900 MHz linearly polarized plane-wave excitation, with the electric field aligned along the wire axis. As shown in Fig. 18 (b), the twisted pair exhibits up to 20 dB lower induced surface current than the parallel pair. It is worth noting that twisted-pair wiring represents one potentially dominant yet not exclusive contributing factor to leakage susceptibility, as PCB traces, power lines and circuit-level nonlinear components also play a role. While it can serve as a useful starting point for mitigation, achieving full immunity requires a comprehensive, security-aware hardware-software co-design approach from the ground up, and we hope this work can inspire future designers to consider such threats early in the design process.

7 Related Work

EM Injection and Side-Channel Leakage. Electromagnetic (EM) security has traditionally evolved along two parallel, non-overlapping paradigms: EM injection and side-channel leakage. EM injection focuses on integrity or availability, where adversaries inject carefully crafted EM signals to induce faults, manipulate sensor output, or disrupt system execution. Recent systematic analysis has shown that EM injection attacks manipulate with multiple stages of cyber-physical system operations, including sensing, computation, actuation, and data communication [25], including critical infrastructure [15, 70, 83], autonomous driving [24, 28, 60, 87], medical healthcare [35, 43], IoT devices [26, 64, 85] and cryptographic modules [21, 22, 48, 53]. Conversely, EM side-channel leakage focuses on integrity or confidentiality, exploiting unintentional EM emanations to recover the cryptographic key of a target device [11, 18, 19] or to reconstruct screen content [32, 33, 72], keystrokes [27], smartphone displays [40], biometric data [37, 52, 81], and even confidential video streams from a smart home camera [41].

Existing research largely treats EM injection and EM side-channel leakage as distinct and independent threat vectors, focusing on fault- and disruption-oriented integrity violations and passive confidentiality threats, respectively. *InjectEave* bridges this gap by theoretically and experimentally showing that EM injections can be used to induce side-channel leakage via hardware nonlinearity, redefining the boundary between active integrity injection attacks and passive confidentiality attacks and enabling closed-loop control capabilities of victim devices. This new attack vector offers significantly enhanced capabilities and generalizability compared to existing state-of-the-art eavesdropping methods. For example, while previous passive EM side channels like *MagEar* [39] and *Periscope* [13] are restricted to 0.5–1.5 m, *InjectEave* can successfully eavesdrop over 30 m. Although *DeHiREC* [88] uses EM injection to augment the strength of weak EMR signals, it primarily amplifies *existing* side-channel leakage (using f_3 to amplify f_1) from ADCs to detect whether a hidden voice recorder is ON/OFF. In contrast, *InjectEave* exploits hardware nonlinearity to induce *entirely new and controllable* side-channel leakage by piggybacking target analog signals f_1 onto an injected carrier f_2 . This different mechanism enables high-fidelity waveform information recovery of continuous analog secrets across diverse electronic components beyond ADCs. Moreover, *InjectEave* offers a substantially broader attack surface; whereas existing studies are often constrained to specific modalities like audio, our approach exploits fundamental vulnerabilities within the analog systems. This makes *InjectEave* modality-agnostic and applicable to a vast spectrum of analog devices.

Contactless Sensing and Backscattering. Contactless sensing and eavesdropping techniques transmit physical signals such as mmWave [8, 23, 38, 66, 75, 76, 80], acous-

tic [14, 20, 61, 62], or optical [46, 51, 63, 74] probing signals, and analyze the resulting reflections to infer information about a target system. However, most of these contactless sensing technologies are so far only able to sense spatial displacements and movements of objects, such as vocal gesture changes [38] and human typing activities [27]. These prior works rely on the existence of nearby vibrating objects. Moreover, optical-based acoustic eavesdropping methods require a clear line of sight, and therefore cannot achieve cross-wall eavesdropping. In contrast, *InjectEave* leverages EM injection and leakage to directly eavesdrop on electrical signals within target circuits, eliminating the dependence on observable physical vibrations and making the attack substantially more robust to environmental movements. Furthermore, the valid EM carrier frequencies, typically in the hundreds-of-MHz range, enable robust through-wall eavesdropping across diverse indoor and outdoor settings.

The closest line of research to *InjectEave* is backscattering communications [29, 58, 84], typically used in low-power RFID systems where a transponder intentionally modulates an RF carrier via impedance switching. Recent research has extended this to unintentional backscattering. Several recent works also exploit binary impedance-modulated backscattering to recover serial communication data [29, 58], or cryptographic side-channel information [30, 49]. However, they rely on a preliminary impedance-variation model that limits these works to binary digital data recovery. Analog signals require fundamentally different theoretical modeling and signal interpretation. In contrast, our work builds upon their insights and limitations, and introduces the first eavesdropping-oriented nonlinear model that enables unprecedented long-distance recovery of analog signals including low-frequency secrets on the order of 10 Hz, exposing an orthogonal, scientifically distinct threat surface, which further enables closed-loop EM eavesdropping and manipulation.

8 Conclusion

This work bridges the theoretical and methodological gap between conventional side-channel analysis and active electromagnetic injection, introducing the novel threat model and analysis framework of Injection-Induced EM Side Channels. By exploiting the ubiquitous nonlinearity in commodity hardware, we demonstrated that adversaries can actively modulate low-frequency analog secrets onto injected carriers before they are efficiently emitted. Our evaluation of 11 commercial devices reveals that this vulnerability is widespread. Our findings underscore an urgent need to develop effective solutions to protect the ubiquitous, but often overlooked, bottom-layer analog interfaces in modern computer systems.

Acknowledgment: This work was supported in part by Guangdong Provincial Key Lab of Integrated Communication, Sensing, and Computation for Ubiquitous Internet of Things (No. 2023B1212010007).

Ethical Considerations

We take strict measures to ensure the safety, legality, and ethical compliance of our research.

Stakeholders and Potential Impact. InjectEave has broad implications across multiple stakeholders. Hardware manufacturers of analog audio interfaces, IoT actuators, and power converters may face pressure to adopt differential signaling or enhanced shielding in future designs. End users face potential privacy risks regarding home activities and private conversations, highlighting the need for greater public awareness of EM security. Finally, InjectEave advances the EM security research community by providing a theoretical framework for injection-induced leakage, motivating the development of active detection systems and robust defenses.

Impact of the Research Process and Publication. All experiments were performed on electronic devices fully controlled by the authors. To strictly protect privacy, we utilized text-to-speech (TTS) tools to synthesize conversation segments for experimentation rather than recording private conversations of human subjects. The “through-wall” and “hotel room” scenarios were conducted in cleared and controlled settings, ensuring no third-party systems or non-consenting individuals were targeted. We believe publishing these results is valuable for manufacturers and defenders seeking to understand the limits of EM side-channel eavesdropping and to investigate possible protections.

Mitigation of Negative Impacts. We have reported these findings to the relevant manufacturers; however, as we have not yet received a response, we have decided to withhold the vulnerable injection frequencies in Table 1 and exclude active injection control logics from our open science artifact. We decided to release this security-sensitive information only to trusted and reputable researchers upon request, restricting our research’s results to scientific exploration. Furthermore, we prioritize defensive insights, demonstrating that twisted-pair wiring serves as a practical countermeasure by effectively suppressing the induced surface currents.

Decision to Conduct and Publish. The historical assumption that low-frequency signals are safe from EM leakage has created a false sense of security. We argue that systematically analyzing this emerging phenomenon of injection-induced EM side channel is essential for building effective defenses. Withholding these findings would leave manufacturers blind to the risks. Therefore, we decided to publish this work while removing detailed attack parameters such as vulnerable EM frequencies, and constraining the majority of the paper to theoretical and defensive insights.

Open Science

Demo videos and audio recordings in case studies are available on our website: <https://injecteave.github.io/>. Our research artifacts, including received audio recordings in

case studies and speech-enhancement codebase are available at: <https://doi.org/10.5281/zenodo.20432240>

References

- [1] TTSMaker – free text to speech online. <https://ttsmaker.com/>. Accessed: 2026-02-05.
- [2] Christian Adami, Christian Braun, Peter Clemens, Michael Suhrke, HU Schmidt, and Achim Taenzer. Hpm detection system for mobile and stationary use. In *10th International Symposium on Electromagnetic Compatibility*, pages 1–6. IEEE, 2011.
- [3] Dakshi Agrawal, Bruce Archambeault, Josyula R Rao, and Pankaj Rohatgi. The em side—channel (s). In *International workshop on cryptographic hardware and embedded systems*, pages 29–45. Springer, 2002.
- [4] Mohammad Abdullah Al Faruque, Sujit Rokka Chhetri, Arquimedes Canedo, and Jiang Wan. Acoustic side-channel attacks on additive manufacturing systems. In *2016 ACM/IEEE 7th international conference on Cyber-Physical Systems (ICCPS)*, pages 1–10. IEEE, 2016.
- [5] Analog Devices. Mt-095: Emi, rfi, and shielding concepts. <https://www.analog.com/media/en/training-seminars/tutorials/MT-095.pdf>, 2009. Accessed: 2026-02-05.
- [6] Anonymous. Injecteave. <https://injecteave.github.io/>, 2026. Accessed: 2026-02-05.
- [7] Michael Backes, Markus Dürmuth, Sebastian Gerling, Manfred Pinkal, Caroline Sporleder, et al. Acoustic {Side-Channel} attacks on printers. In *19th USENIX Security Symposium (USENIX Security 10)*, 2010.
- [8] Suryoday Basak and Mahanth Gowda. mmspy: Spying phone calls using mmwave radars. In *2022 IEEE Symposium on Security and Privacy (SP)*, pages 1211–1228. IEEE, 2022.
- [9] Connor Bolton, Yan Long, Jun Han, Josiah Hester, and Kevin Fu. Characterizing and mitigating touchtone eavesdropping in smartphone motion sensors. In *Proceedings of the 26th International Symposium on Research in Attacks, Intrusions and Defenses*, pages 164–178, 2023.
- [10] Elie Bursztein, Luca Invernizzi, Karel Král, Daniel Moghimi, Jean-Michel Picod, and Marina Zhang. Generalized power attacks against crypto hardware using long-range deep learning. *arXiv preprint arXiv:2306.07249*, 2023.

- [11] Giovanni Camurati, Sebastian Poeplau, Marius Muench, Tom Hayes, and Aurélien Francillon. Screaming channels: When electromagnetic side channels meet radio transceivers. In *Proceedings of the 2018 ACM SIGSAC Conference on Computer and Communications Security*, pages 163–177, 2018.
- [12] Anantha P Chandrakasan, Samuel Sheng, and Robert W Brodersen. Low-power cmos digital design. *IEICE Transactions on Electronics*, 75(4):371–382, 1992.
- [13] Huiling Chen, Wenqiang Jin, Yupeng Hu, Zhenyu Ning, Kenli Li, Zheng Qin, Mingxing Duan, Yong Xie, Daibo Liu, and Ming Li. Eavesdropping on black-box mobile devices via audio amplifier’s emr. In *Proceedings of the NDSS 2018*, 2024.
- [14] Peng Cheng, Ibrahim Ethem Bagci, Utz Roedig, and Jeff Yan. Sonarsnoop: Active acoustic side-channel attacks. *International Journal of Information Security*, 19(2):213–228, 2020.
- [15] Benjamin Cyr, Yan Long, Takeshi Sugawara, and Kevin Fu. Position paper: Space system threat models must account for satellite sensor spoofing. In *SpaceSec*, 2023.
- [16] Matt Ettus and Martin Braun. The universal software radio peripheral (usrp) family of low-cost sdrs. *Opportunistic spectrum sharing and white space access: The practical reality*, pages 3–23, 2015.
- [17] Julie Ferrigno and Martin Hlaváč. When aes blinks: introducing optical side channel. *IET Information Security*, 2(3):94–98, 2008.
- [18] Daniel Genkin, Lev Pachmanov, Itamar Pipman, and Eran Tromer. Stealing keys from pcs using a radio: Cheap electromagnetic attacks on windowed exponentiation. In *International workshop on cryptographic hardware and embedded systems*, pages 207–228. Springer, 2015.
- [19] Dennis RE Gnad, Jonas Krautter, and Mehdi B Tahoori. Leaky noise: New side-channel attack vectors in mixed-signal iot devices. *IACR Transactions on Cryptographic Hardware and Embedded Systems*, pages 305–339, 2019.
- [20] Tzipora Halevi and Nitesh Saxena. Keyboard acoustic side channel attacks: exploring realistic and security-sensitive scenarios. *International Journal of Information Security*, 14(5):443–456, 2015.
- [21] Yu-ichi Hayashi, Naofumi Homma, Takaaki Mizuki, Takafumi Aoki, and Hideaki Sone. Transient iemi threats for cryptographic devices. *IEEE transactions on Electromagnetic Compatibility*, 55(1):140–148, 2012.
- [22] Yu-ichi Hayashi, Naofumi Homma, Takaaki Mizuki, Takafumi Aoki, and Hideaki Sone. Precisely timed iemi fault injection synchronized with em information leakage. In *2014 IEEE International Symposium on Electromagnetic Compatibility (EMC)*, pages 738–742. IEEE, 2014.
- [23] Pengfei Hu, Yifan Ma, Panneer Selvam Santhalingam, Parth H Pathak, and Xiuzhen Cheng. Milliar: Millimeter-wave acoustic eavesdropping with unconstrained vocabulary. In *IEEE INFOCOM 2022-IEEE Conference on Computer Communications*, pages 11–20. IEEE, 2022.
- [24] Qinhong Jiang, Xiaoyu Ji, Chen Yan, Zhixin Xie, Haina Lou, and Wenyan Xu. {GlitchHiker}: Uncovering vulnerabilities of image signal transmission with {IEMI}. In *32nd USENIX Security Symposium (USENIX Security 23)*, pages 7249–7266, 2023.
- [25] Qinhong Jiang, Yan Long, Youqian Zhang, Chen Yan, Xiaoyu Ji, Xiapu Luo, Kevin Fu, Jiannong Cao, and Wenyan Xu. Sok: Security of cyber-physical systems under intentional electromagnetic interference attacks. In *35th USENIX Security Symposium (USENIX Security 26)*, 2026.
- [26] Qinhong Jiang, Yanze Ren, Yan Long, Chen Yan, Yumai Sun, Xiaoyu Ji, Kevin Fu, and Wenyan Xu. Ghosttype: The limits of using contactless electromagnetic interference to inject phantom keys into analog circuits of keyboards. In *NDSS Symposium*. Internet Society, 2024.
- [27] Wenqiang Jin, Srinivasan Murali, Huadi Zhu, and Ming Li. Periscope: A keystroke inference attack using human coupled electromagnetic emanations. In *Proceedings of the 2021 ACM SIGSAC Conference on Computer and Communications Security*, pages 700–714, 2021.
- [28] Zizhi Jin, Qinhong Jiang, Xuancun Lu, Chen Yan, Xiaoyu Ji, and Wenyan Xu. Phantomlidar: Cross-modality signal injection attacks against lidar. In *NDSS Symposium*. Internet Society, 2025.
- [29] Shugo Kaji, Daisuke Fujimoto, Masahiro Kinugawa, and Yuichi Hayashi. Echo tempest: Em information leakage induced by iemi for electronic devices. *IEEE Transactions on Electromagnetic Compatibility*, 65(3):655–666, 2023.
- [30] Taiki Kitazawa, Lennert Wouters, Benedikt Gierlichs, Daisuke Fujimoto, Ingrid Verbauwhede, and Yuichi Hayashi. Active electromagnetic side-channel analysis: Crossing physical security boundaries through impedance variations. *IACR Transactions on Cryptographic Hardware and Embedded Systems*, 2026(1):376–401, 2026.

- [31] D Richard Kuhn, Thomas J Walsh, and Steffen Fries. Security considerations for voice over ip systems. *NIST special publication*, 800, 2005.
- [32] Markus G Kuhn. Optical time-domain eavesdropping risks of crt displays. In *Proceedings 2002 IEEE Symposium on Security and Privacy*, pages 3–18. IEEE, 2002.
- [33] Markus G Kuhn. Electromagnetic eavesdropping risks of flat-panel displays. In *International Workshop on Privacy Enhancing Technologies*, pages 88–107. Springer, 2004.
- [34] Markus G Kuhn and Ross J Anderson. Soft tempest: Hidden data transmission using electromagnetic emanations. In *International Workshop on Information Hiding*, pages 124–142. Springer, 1998.
- [35] Denis Foo Kune, John Backes, Shane S Clark, Daniel Kramer, Matthew Reynolds, Kevin Fu, Yongdae Kim, and Wenyan Xu. Ghost talk: Mitigating emi signal injection attacks against analog sensors. In *2013 IEEE symposium on security and privacy*. IEEE, 2013.
- [36] Jiachun Li, Yan Meng, Le Zhang, Guoxing Chen, Yuan Tian, Haojin Zhu, and Xuemin Sherman Shen. Magfingerprint: A magnetic based device fingerprinting in wireless charging. In *IEEE INFOCOM 2023-IEEE Conference on Computer Communications*, pages 1–10. IEEE, 2023.
- [37] Wenhao Li, Jiahao Wang, Guoming Zhang, Yanni Yang, Riccardo Spolaor, Xiuzhen Cheng, and Pengfei Hu. Emiris: Eavesdropping on iris information via electromagnetic side channel. In *Network and Distributed Systems Security (NDSS) Symposium*. Internet Society, 2025.
- [38] Zhengxiong Li, Fenglong Ma, Aditya Singh Rathore, Zhuolin Yang, Baicheng Chen, Lu Su, and Wenyan Xu. Wavespy: Remote and through-wall screen attack via mmwave sensing. In *2020 IEEE Symposium on Security and Privacy (SP)*, pages 217–232. IEEE, 2020.
- [39] Qianru Liao, Yongzhi Huang, Yandao Huang, Yuheng Zhong, Huitong Jin, and Kaishun Wu. Magear: eavesdropping via audio recovery using magnetic side channel. In *MobiSys*, pages 371–383, 2022.
- [40] Zhuoran Liu, Niels Samwel, Léo Weissbart, Zhengyu Zhao, Dirk Lauret, Lejla Batina, and Martha Larson. Screen gleanig: A screen reading tempest attack on mobile devices exploiting an electromagnetic side channel. In *Proceedings of the 28th Annual Network and Distributed System Security Symposium (NDSS)*, 2021.
- [41] Yan Long, Qinhong Jiang, Chen Yan, Tobias Alam, Xiaoyu Ji, Wenyan Xu, and Kevin Fu. Em eye: Characterizing electromagnetic side-channel eavesdropping on embedded cameras. In *Network and Distributed Systems Security (NDSS) Symposium*. Internet Society, 2024.
- [42] Yan Long, Pirouz Naghavi, Blas Kojusner, Kevin Butler, Sara Rampazzi, and Kevin Fu. Side eye: Characterizing the limits of pov acoustic eavesdropping from smartphone cameras with rolling shutters and movable lenses. In *2023 IEEE symposium on security and privacy (SP)*, pages 1857–1874. IEEE, 2023.
- [43] Yan Long, Sara Rampazzi, Takeshi Sugawara, and Kevin Fu. Protecting covid-19 vaccine transportation and storage from analog cybersecurity threats. *Biomedical Instrumentation & Technology*, 55(3):112–117, 2021.
- [44] Yan Long, Chen Yan, Shilin Xiao, Shivan Prasad, Wenyan Xu, and Kevin Fu. Private eye: On the limits of textual screen peeking via eyeglass reflections in video conferencing. In *2023 IEEE Symposium on Security and Privacy (SP)*, pages 3432–3449. IEEE, 2023.
- [45] Joe Loughry and David A Umphress. Information leakage from optical emanations. *ACM Transactions on Information and System Security (TISSEC)*, 5(3):262–289, 2002.
- [46] Chengwen Luo, Zhuoqing Xie, Yuhan Huang, Gecheng Chen, Haiyi Yao, Jin Zhang, Long Cheng, Weitao Xu, and Jianqiang Li. Laserkey: Eavesdropping keyboard typing leveraging vibrational emanations via laser sensing. *IEEE Transactions on Mobile Computing*, 2025.
- [47] Seita Maruyama, Satohiro Wakabayashi, and Tatsuya Mori. Tap’n ghost: A compilation of novel attack techniques against smartphone touchscreens. In *2019 IEEE Symposium on Security and Privacy (SP)*, pages 620–637. IEEE, 2019.
- [48] Alexandre Menu, Jean-Max Dutertre, Olivier Potin, Jean-Baptiste Rigaud, and Jean-Luc Danger. Experimental analysis of the electromagnetic instruction skip fault model. In *15th Design & Technology of Integrated Systems in Nanoscale Era (DTIS)*, pages 1–7. IEEE, 2020.
- [49] Saleh Khalaj Monfared, Tahoura Mosavirik, and Shahin Tajik. Leakyohm: Secret bits extraction using impedance analysis. In *Proceedings of the 2023 ACM SIGSAC conference on computer and communications security*, pages 1675–1689, 2023.
- [50] Pouya Narimani, Meng Wang, Ulysse Planta, and Ali Abbasi. Exploring power side-channel challenges in embedded systems security. *arXiv preprint arXiv:2410.11563*, 2024.

- [51] Ben Nassi, Raz Swissa, Jacob Shams, Boris Zadov, and Yuval Elovici. The little seal bug: Optical sound recovery from lightweight reflective objects. In *2023 IEEE Security and Privacy Workshops (SPW)*, pages 298–310. IEEE, 2023.
- [52] Tao Ni, Xiaokuan Zhang, and Qingchuan Zhao. Recovering fingerprints from in-display fingerprint sensors via electromagnetic side channel. In *Proceedings of the 2023 ACM SIGSAC Conference on Computer and Communications Security*, pages 253–267, 2023.
- [53] Hikaru Nishiyama, Daisuke Fujimoto, and Yuichi Hayashi. Remote fault injection attack against cryptographic modules via intentional electromagnetic interference from an antenna. In *2023 Workshop on Attacks and Solutions in Hardware Security*, 2023.
- [54] Arifu Onishi, S Hrushikesh Bhupathiraju, Rishikesh Bhatt, Sara Rampazzi, and Takeshi Sugawara. Sound of interference: Electromagnetic eavesdropping attack on digital microphones using pulse density modulation. In *34th USENIX Security Symposium (USENIX Security 25)*, pages 3865–3884, 2025.
- [55] Henry W Ott. *Electromagnetic compatibility engineering*. John Wiley & Sons, 2011.
- [56] Vassil Panayotov, Guoguo Chen, Daniel Povey, and Sanjeev Khudanpur. Librispeech: an asr corpus based on public domain audio books. In *Acoustics, Speech and Signal Processing (ICASSP), 2015 IEEE International Conference on*, pages 5206–5210. IEEE, 2015.
- [57] Karl S Pearsons, Ricarda L Bennett, and Sanford A Fiddell. *Speech levels in various noise environments*. Office of Health and Ecological Effects, Office of Research and Development . . . , 1977.
- [58] Lina Pu, Yu Luo, Song Han, and Junming Diao. Your cable, my antenna: Eavesdropping serial communication via backscatter signals. In *2025 IEEE Symposium on Security and Privacy (SP)*, pages 3710–3726. IEEE Computer Society, 2025.
- [59] Alec Radford, Jong Wook Kim, Tao Xu, Greg Brockman, Christine McLeavey, and Ilya Sutskever. Robust speech recognition via large-scale weak supervision. In *Proceedings of the 40th International Conference on Machine Learning*, pages 28492–28518, 2023.
- [60] Yanze Ren, Qinhong Jiang, Chen Yan, Xiaoyu Ji, and Wenyuan Xu. Ghostshot: Manipulating the image of ccd cameras with electromagnetic interference. In *NDSS Symposium*. Internet Society, 2025.
- [61] Yanzhi Ren, Zhiliang Xia, Siyi Li, Hongbo Liu, Yingying Chen, Shuai Li, and Hongwei Li. Echoimage: User authentication on smart speakers using acoustic signals. In *2023 IEEE 43rd International Conference on Distributed Computing Systems (ICDCS)*, pages 236–247. IEEE, 2023.
- [62] Nirupam Roy and Romit Roy Choudhury. Listening through a vibration motor. In *Proceedings of the 14th Annual International Conference on Mobile Systems, Applications, and Services*, pages 57–69, 2016.
- [63] Sriram Sami, Yimin Dai, Sean Rui Xiang Tan, Nirupam Roy, and Jun Han. Spying with your robot vacuum cleaner: eavesdropping via lidar sensors. In *Proceedings of the 18th Conference on Embedded Networked Sensor Systems*, pages 354–367, 2020.
- [64] Haoqi Shan, Boyi Zhang, Zihao Zhan, Dean Sullivan, Shuo Wang, and Yier Jin. Invisible finger: Practical electromagnetic interference attack on touchscreen-based electronic devices. In *2022 IEEE Symposium on Security and Privacy (SP)*. IEEE, 2022.
- [65] François-Xavier Standaert. Introduction to side-channel attacks. In *Secure integrated circuits and systems*, pages 27–42. Springer, 2009.
- [66] Wei Sun, Tingjun Chen, and Neil Gong. Sok: Secure human-centered wireless sensing. *arXiv preprint arXiv:2211.12087*, 2022.
- [67] Marcell Szakály, Sebastian Köhler, Martin Strohmeier, and Ivan Martinovic. Assault and battery: Evaluating the security of power conversion systems against electromagnetic injection attacks. In *2024 Annual Computer Security Applications Conference (ACSAC)*, pages 224–239. IEEE, 2024.
- [68] David Tse and Pramod Viswanath. *Fundamentals of wireless communication*. Cambridge university press, 2005.
- [69] Yazhou Tu, Zhiqiang Lin, Insup Lee, and Xiali Hei. Injected and delivered: Fabricating implicit control over actuation systems by spoofing inertial sensors. In *27th USENIX security symposium (USENIX Security 18)*, pages 1545–1562, 2018.
- [70] Yazhou Tu, Sara Rampazzi, Bin Hao, Angel Rodriguez, Kevin Fu, and Xiali Hei. Trick or heat?: Manipulating critical temperature-based control systems using rectification attacks. In *2019 ACM SIGSAC Conference on Computer and Communications Security*.
- [71] Yazhou Tu, Vijay Srinivas Tida, Zhongqi Pan, and Xiali Hei. Transduction shield: A low-complexity method to detect and correct the effects of emi injection attacks on

- sensors. In *Proceedings of the 2021 ACM Asia Conference on Computer and Communications Security*, pages 901–915, 2021.
- [72] Wim Van Eck. Electromagnetic Radiation from Video Display Units: An Eavesdropping Risk? *Computers & Security*, 4(4):269–286, 1985.
- [73] Martin Vuagnoux and Sylvain Pasini. Compromising electromagnetic emanations of wired and wireless keyboards. In *Proceedings of the 18th USENIX Conference on Security Symposium*, volume 8, pages 1–16, 2009.
- [74] Payton Walker and Nitesh Saxena. Laser meager listener: A scientific exploration of laser-based speech eavesdropping in commercial user space. In *2022 IEEE 7th European Symposium on Security and Privacy (EuroS&P)*, pages 537–554. IEEE, 2022.
- [75] Chao Wang, Feng Lin, Tiantian Liu, Ziwei Liu, Yijie Shen, Zhongjie Ba, Li Lu, Wenyao Xu, and Kui Ren. mmphone: Acoustic eavesdropping on loudspeakers via mmwave-characterized piezoelectric effect. In *IEEE INFOCOM 2022-IEEE Conference on Computer Communications*, pages 820–829. IEEE, 2022.
- [76] Chao Wang, Feng Lin, Tiantian Liu, Kaidi Zheng, Zhibo Wang, Zhengxiong Li, Ming-Chun Huang, Wenyao Xu, and Kui Ren. mmeve: eavesdropping on smartphone’s earpiece via cots mmwave device. In *Proceedings of the 28th Annual International Conference on Mobile Computing And Networking*, pages 338–351, 2022.
- [77] Kai Wang, Richard Mitev, Chen Yan, Xiaoyu Ji, Ahmad-Reza Sadeghi, and Wenyuan Xu. {GhostTouch}: Targeted attacks on touchscreens without physical touch. In *31st USENIX Security Symposium (USENIX Security 22)*, 2022.
- [78] Simon Welker, Julius Richter, and Timo Gerkmann. Speech enhancement with score-based generative models in the complex STFT domain. In *Proc. Interspeech 2022*, pages 2928–2932, 2022.
- [79] Harold A Wheeler. Fundamental limitations of small antennas. *Proceedings of the IRE*, 35(12):1479–1484, 2006.
- [80] Chenhan Xu, Zhengxiong Li, Hanbin Zhang, Aditya Singh Rathore, Huining Li, Chen Song, Kun Wang, and Wenyao Xu. Waveear: Exploring a mmwave-based noise-resistant speech sensing for voice-user interface. In *Proceedings of the 17th MobiSys*, pages 14–26, 2019.
- [81] Haowen Xu, Tianya Zhao, Xuyu Wang, Lei Ma, Jun Dai, Alexander Wyglinski, and Xiaoyan Sun. Empalm: Exfiltrating palm biometric data via electromagnetic side-channel. In *Proceedings of the 2026 ACM/IEEE International Conference on Embedded Artificial Intelligence and Sensing Systems*, pages 1043–1056, 2026.
- [82] Zhifei Xu, Runbing Hua, Jack Juang, Shengxuan Xia, Jun Fan, and Chulsoon Hwang. Inaudible attack on smart speakers with intentional electromagnetic interference. *IEEE Transactions on Microwave Theory and Techniques*, 69(5):2642–2650, 2021.
- [83] Fengchen Yang, Zihao Dan, Kaikai Pan, Chen Yan, Xiaoyu Ji, and Wenyuan Xu. Rethink: Reveal the threat of electromagnetic interference on power inverters. In *NDSS Symposium*. Internet Society, 2025.
- [84] Yanni Yang, Genglin Wang, Zhenlin An, Guoming Zhang, Xiuzhen Cheng, and Pengfei Hu. Rf-parrot: Wireless eavesdropping on wired audio. In *IEEE INFOCOM 2024-IEEE Conference on Computer Communications*, pages 701–710. IEEE, 2024.
- [85] Xingli Zhang, Yazhou Tu, Yan Long, Liqun Shan, Mohamed A Elsaadani, Kevin Fu, Zhiqiang Lin, and Xiali Hei. From virtual touch to tesla command: Unlocking unauthenticated control chains from smart glasses for vehicle takeover. In *2024 IEEE Symposium on Security and Privacy (SP)*, pages 201–201. IEEE, 2024.
- [86] Youqian Zhang and Kasper Rasmussen. Detection of electromagnetic interference attacks on sensor systems. In *2020 IEEE Symposium on Security and Privacy (SP)*, pages 203–216. IEEE, 2020.
- [87] Youqian Zhang, Chunxi Yang, Eugene Y Fu, Qinlong Jiang, Chen Yan, Sze-Yiu Chau, Grace Ngai, Hong-Va Leong, Xiapu Luo, and Wenyuan Xu. Understanding impacts of electromagnetic signal injection attacks on object detection. In *2024 IEEE International Conference on Multimedia and Expo (ICME)*, pages 1–6. IEEE, 2024.
- [88] Ruochen Zhou, Xiaoyu Ji, Chen Yan, Yi-Chao Chen, Wenyuan Xu, and Chaohao Li. Dehirec: Detecting hidden voice recorders via adc electromagnetic radiation. In *2023 IEEE Symposium on Security and Privacy (SP)*, pages 3113–3128. IEEE, 2023.
- [89] Siyi Zhou, Yiquan Zhou, Yi He, Xun Zhou, Jinchao Wang, Wei Deng, and Jingchen Shu. Indextts2: A breakthrough in emotionally expressive and duration-controlled auto-regressive zero-shot text-to-speech. *arXiv preprint arXiv:2506.21619*, 2025.
- [90] Hui Zhuang, Yan Long, and Kevin Fu. Rf-eye-d: Probing feasibility of cmos camera watermarking with radio-frequency injection. In *the 28th RAID*, 2025.